Early T cell receptor signals globally modulate ligand: receptor affinities during antigen discrimination

Rafal M. Pielak[a,1,2], Geoff P. O'Donoghue[a,1,3], Jenny J. Lin[a,1], Katherine N. Alfieri[a,4], Nicole C. Fay[a,b,5], Shalini T. Low-Nam[a], and Jay T. Groves[a,6]

[a]Department of Chemistry, University of California, Berkeley, CA 94720; and [b]Department of Molecular and Cellular Biology, University of California, Berkeley, CA 94720

Edited by Ronald N. Germain, National Institutes of Health, Bethesda, MD, and approved August 28, 2017 (received for review August 7, 2016)

Antigen discrimination by T cells occurs at the junction between a T cell and an antigen-presenting cell. Juxtacrine binding between numerous adhesion, signaling, and costimulatory molecules defines both the topographical and lateral geometry of this cell–cell interface, within which T cell receptor (TCR) and peptide major histocompatibility complex (pMHC) interact. These physical constraints on receptor and ligand movement have significant potential to modulate their molecular binding properties. Here, we monitor individual ligand:receptor binding and unbinding events in space and time by single-molecule imaging in live primary T cells for a range of different pMHC ligands and surface densities. Direct observations of pMHC:TCR and CD80:CD28 binding events reveal that the in situ affinity of both pMHC and CD80 ligands for their respective receptors is modulated by the steady-state number of agonist pMHC:TCR interactions experienced by the cell. By resolving every single pMHC:TCR interaction it is evident that this cooperativity is accomplished by increasing the kinetic on-rate without altering the off-rate and has a component that is not spatially localized. Furthermore, positive cooperativity is observed under conditions where the T cell activation probability is low. This TCR-mediated feedback is a global effect on the intercellular junction. It is triggered by the first few individual pMHC:TCR binding events and effectively increases the efficiency of TCR scanning for antigen before the T cell is committed to activation.

single-molecule ligand:receptor assay | T cell receptor | peptide discrimination | signal transduction | immune synapse

T cell activation in the adaptive immune system is mediated by ligand:receptor interactions at the interface between a T cell and an antigen-presenting cell (APC). T cells are known to be extremely sensitive (1, 2) and have even been reported to trigger and produce cytokines in response to even a single peptide major histocompatibility complex (pMHC) ligand (3). T cells are also highly selective and can accurately discriminate between different pMHCs based on small differences in molecular binding properties—especially the kinetic dissociation rate (k_{off}) of the pMHC: T cell receptor (TCR) complex (4–9). The fundamental problem faced by any system that has both single-molecule sensitivity and precise discrimination is that molecular properties such as k_{off} are intrinsically ensemble averages. At the single-molecule level, each pMHC:TCR interaction consists of a discrete dwell time (τ_{off}), and k_{off} is only defined as $1/\langle\tau_{off}\rangle$ for a large number of events. Individual values of τ_{off} for pMHC:TCR binding events are roughly exponentially distributed and even a weakly binding agonist will occasionally remain bound much longer than average (10–12). Although hypotheses have been put forward, the basic question of how a T cell distinguishes the rare, genuine agonist pMHC from spurious long-lived complexes with the abundant self pMHC is not resolved (13–17).

Here, we monitor the spatial position and temporal duration of all molecular pMHC:TCR binding events during T cell antigen discrimination. Measurements are made using hybrid live T cell–supported membrane junctions, which enable controlled presentation of antigen pMHC in the context of adhesion and costimulatory molecules, all in a fluid environment that mimics many properties of a cell–cell interface (18–20). The binding state of each individual pMHC molecule is resolved based on single-molecule tracking of its lateral mobility, providing a real-time readout of the binding status of every pMHC within the junction (12).

Two key molecular binding parameters are directly revealed by these measurements: the pMHC:TCR dwell time distribution and the fraction of pMHC actually bound to TCR under each cell. The molecular dwell time distribution (related to the in situ kinetic off-rate) was observed to remain constant over a wide range of conditions. However, the fraction of bound pMHC (related to the in situ dissociation constant) exhibited distinct positive feedback at the lowest antigen densities. Progressive accumulation of antigen pMHC:TCR interactions globally increases the affinity of pMHC for TCR throughout the interface. This cooperativity occurs over micrometer distances and is thus not based on physical contact between pMHC:TCR complexes. Cooperativity is instead mediated through changes in the kinetic on-rate (k_{on}), which result from global changes in the geometry of the cell–cell interface induced by early TCR signaling events. Single-molecule imaging of costimulatory CD80:CD28 binding reveals that these environmental changes also increase the binding efficiency of other ligand:receptor interactions in the

Significance

Antigen discrimination by T cells is based on subtle differences in binding of the T cell receptor (TCR) for its peptide major histocompatibility complex (pMHC) ligand. While such binding characteristics are readily mapped with great precision in reconstituted biochemical systems, it is less clear how these interactions are affected in the live cell environment. Here we utilize single-molecule imaging to individually resolve all of the pMHC:TCR binding events in live T cells. The quantitative measurements reveal an active feedback mechanism that globally modulates the probability of pMHC:TCR binding throughout the cell–cell interface, without affecting the unbinding rate. The result is to increase the efficiency with which TCRs scan for antigen pMHC after the first few molecular encounters have occurred.

Author contributions: R.M.P., G.P.O., J.J.L., N.C.F., S.T.L.-N., and J.T.G. designed research; R.M.P., G.P.O., J.J.L., K.N.A., and S.T.L.-N. performed research; R.M.P., G.P.O., J.J.L., K.N.A., N.C.F., and S.T.L.-N. contributed new reagents/analytic tools; R.M.P., G.P.O., J.J.L., K.N.A., S.T.L.-N., and J.T.G. analyzed data; and R.M.P., G.P.O., J.J.L., and J.T.G. wrote the paper.

The authors declare no conflict of interest.

This article is a PNAS Direct Submission.

[1]R.M.P., G.P.O., and J.J.L. contributed equally to this work.

[2]Present address: L'Oréal Tech Incubator, San Francisco, CA 94105.

[3]Present address: Department of Cellular and Molecular Pharmacology, University of San Francisco, San Francisco, CA 94158.

[4]Present address: Stanford ChEM-H, Stanford University, Stanford, CA 94305.

[5]Present address: Applied Molecular Transport, South San Francisco, CA 94080.

[6]To whom correspondence should be addressed. Email: jtgroves@lbl.gov.

This article contains supporting information online at www.pnas.org/lookup/suppl/doi:10.1073/pnas.1613140114/-/DCSupplemental.

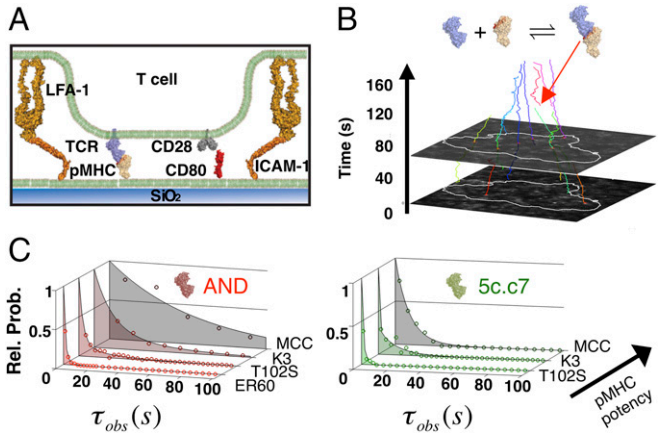

Fig. 1. Monitoring single-molecule ligand:receptor binding events in living T cells. (*A*) Single-cell responses of T cells to TCR triggering are probed in hybrid interfaces between live T cells and supported membranes functionalized with receptor ligands (pMHC and CD80) and adhesion molecules [the integrin ligand ICAM-1, Protein Data Bank (PDB) ID code 1IAM and 1P53]. The kinetics and stoichiometry of pMHC:TCR (PDB ID code 3QIU) and CD80:CD28 (PDB ID code 1DR9 and 1YJD) are monitored using total internal reflectance (TIRF) microscopy, where bright organic fluorophores covalently coupled to the ligand (either pMHC or CD80) are used as high-contrast imaging agents. ICAM-YFP, which binds its receptor LFA-1 (PDB ID codes 2K9J and 3K72), is imaged using TIRF to observe adhesion organization. NFAT-GFP nuclear localization and ZAP70-EGFP membrane localization report on the signaling status of living T cells in response to pMHC stimulation. (*B*) A representative time lapse of single-molecule MCC/MHC:AND trajectories. Each color represents a different pMHC:TCR single-molecule trajectory lasting tens to hundreds of seconds. Trajectories beginning at later time points (red arrow) represent de novo ligand:receptor binding events. (*C*) The distribution of single-molecule pMHC:TCR dwell times (τ_{off}) is measured for different pMHC:TCR combinations. Hundreds of molecular traces from ≥10 cells are used to populate each distribution, with fits shown. In general, higher-potency pMHC ligands have longer $\langle\tau_{off}\rangle$. pMHC:TCR $\langle\tau_{off}\rangle$ were measured with a 500-ms camera exposure time and time-lapse intervals varying between 1 s and 10 s.

interface. Inside-out activation of lymphocyte function associated antigen-1 (LFA-1) on the T cell surface (21) and changes in the cortical actin cytoskeleton (18, 22) are plausible candidates for such feedback. Notably, positive cooperativity is only observed at pMHC densities where T cells are unlikely to be activated (e.g., as measured by NFAT nuclear translocation in these experiments). At progressively higher antigen levels, corresponding to conditions under which central supramolecular activation clusters are clearly visible (23), the observed cooperativity becomes negative.

These observations expose active feedback through the TCR signaling network that modulates pMHC:TCR and other molecular binding affinities in situ. One consequence of this feedback is to increase the efficiency with which TCRs scan for pMHC after the first few agonist pMHC:TCR molecular binding events have occurred, but before the decision to activate is reached. The sensitivity of the feedback mechanism to antigen thus even exceeds the already extreme sensitivity with which T cells activate in response to antigen. Another consequence of such a feedback system is to increase the probability of multiply rebinding the same agonist pMHC (24). Under situations where extremely few or even a single agonist pMHC is available, multiple rebinding events increase the precision with which molecular properties of the agonist, such as the corresponding pMHC:TCR k_{off}, can be determined. Feedback that favors multiple rebinding events will thus increase the ability of TCR to discriminate among similar pMHCs based on binding kinetics. More generally, these observations underscore how chemical properties, such as binding affinities, can be dynamically manipulated in the living cellular environment.

Results

Single-Molecule pMHC:TCR Binding in Live Cells. We probe single T cell responses to TCR triggering in hybrid junctions between live primary T cells and supported lipid membranes functionalized with pMHC, the integrin intracellular adhesion molecule-1 (ICAM-1), and the costimulatory ligand CD80 (Fig. 1*A*). T cells spread rapidly via integrin binding to form essentially planar interfaces with the supported membrane. As reported previously (12), individual pMHC:TCR complexes can be tracked in these hybrid junctions by taking advantage of the dramatic decrease in mobility of pMHC bound to TCR in the T cell plasma membrane relative to pMHC diffusing freely in the supported membrane (Fig. 1*B*). Using this approach we tracked slow-moving, bound pMHC:TCR complexes and measured the single-molecule pMHC:TCR dwell time distributions for two different TCR mouse model systems (AND and 5c.c7) and a panel of peptide ligands of varying potencies (Fig. 1*C*). The average molecular dwell times ($\langle\tau_{off}\rangle$) range from <1 s to 68 s, correlate with observed peptide potency in these studies, and are

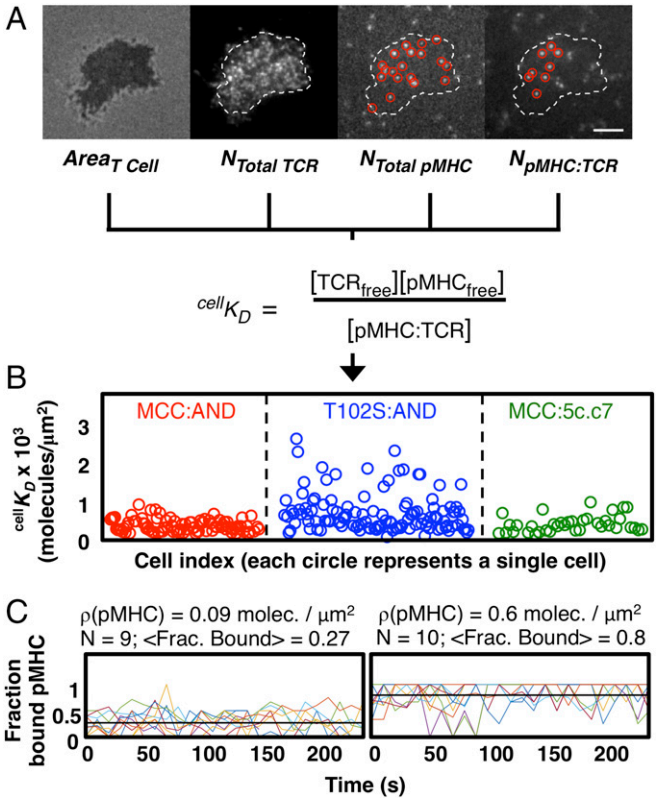

Fig. 2. Direct, single-molecule calculation of pMHC:TCR dissociation quotients. (*A*) Sequential 500-ms and 40-ms acquisitions, respectively, record the number of bound pMHC (from the 500-ms acquisition) and the total number of pMHC ligand molecules (from the 40-ms acquisition) per individual T cell. Cell outline is determined using reflection interference contrast microscopy (RICM). Representative images are from an AND T cell interacting with 0.09 molecules per micrometer MCC/MHC. Subsequent measurement of the total number of TCR in the live cell-supported membrane interface via TIRF enables calculation of pMHC:TCR K_D on a single cell basis, ${}^{cell}K_D$. (Scale bar, 5 μm.) (*B*) ${}^{cell}K_D$ is measured at the single-molecule, single-cell level for the MCC/MHC:AND, T102S/MHC:AND, and MCC/MHC:5c.c7 pMHC:TCR combinations. Each circle represents a cell. Higher-potency ligands correspond with higher-affinity pMHC:TCR interactions. The pMHC density for these data sets are ~50–300 pMHC per micrometer, ~50–300 pMHC per micrometer, and 125 and 340 pMHC per micrometer for the MCC:AND, T102S:AND, and MCC:5c.c7 combinations, respectively. (*C*) Single-cell kinetic traces of fraction bound pMHC at two different MCC densities (0.09 and 0.6 μm^{-2}) using AND T cells. All traces begin after 5 min of initial cell landing. Each colored line represents one cell. The black line indicates the steady-state mean. pMHCs are labeled 1:1 with Atto488 for all experiments.

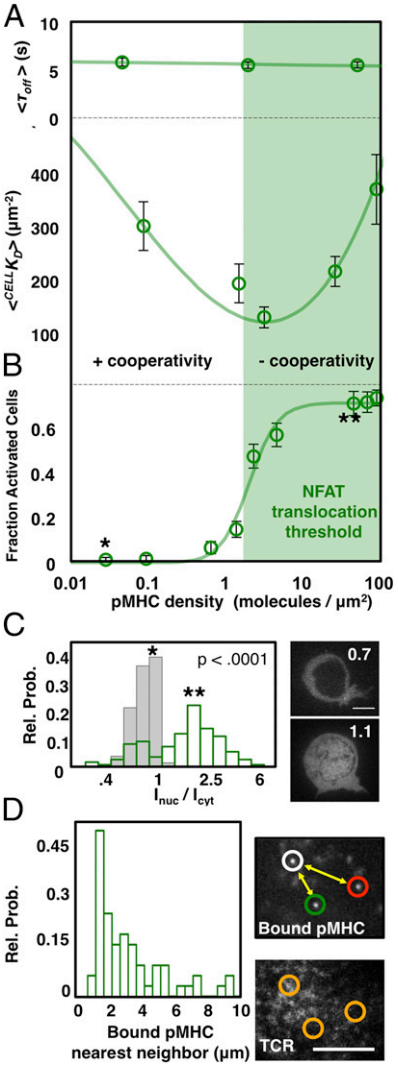

Fig. 3. ${}^{cell}K_D$ varies regularly with ligand density. (*A*, *Top*) $\langle\tau_{off}\rangle$ remains constant during a pMHC density titration over almost four orders of magnitude in the supported membrane. (*A*, *Bottom*) Over the same pMHC density range, $\langle {}^{cell}K_D\rangle$, measured using the single-molecule, single-cell assay demonstrated in Fig. 2, varies regularly, reaching an optimum at low pMHC densities. pMHC:TCR binding exhibits positive cooperativity at low ligand densities (corresponding to as few as five steady-state pMHC:TCR binding events) until reaching the optimal pMHC density. At values higher than optimal pMHC density, pMHC:TCR binding exhibits negative cooperativity. (*B*) NFAT translocation thresholds correspond with pMHC:TCR binding optimums. All data in *A* and *B* were recorded using the MCC/MHC:5c.c7 pMHC:TCR combination. Each circle indicates a population average, and error bars show SEM. $n \geq 50$ for ${}^{cell}K_D$ and NFAT measurements at each condition, and kinetic measurements were performed as in Fig. 1. All data are representative of at least three biological replicates. (*C*) NFAT translocation is measured on a cell-by-cell basis by calculating the degree of NFAT-GFP nuclear localization within a 500-nm-thick optical section (obtained using spinning disk confocal microscopy) from the middle of the T cell. If the ratio of nuclear to cytosolic NFAT-GFP intensity (I_{nuc}/I_{cyt}) is greater than 1, then that T cell is defined as activated. Numbers in upper right of the two images at right indicate the I_{nuc}/I_{cyt} value for the cells shown. (*D*, *Left*) The distribution of bound pMHC nearest neighbors was calculated for the MCC:5c.c7 interaction at 0.1 MCC/μm^2. * and ** correspond to the pMHC densities depicted in *B*. (*D*, *Right*) Schematic of the nearest-neighbor calculation. The MCC outlined in green is the nearest neighbor of the MCC outlined in white. An image of TCR (labeled using H57 Fab conjugated to Alexa647) from the same cell demonstrates that TCR density is not locally increased at sites of pMHC binding. (All scale bars, 5 μm.)

comparable to reported bulk solution binding measurements on isolated proteins made using surface plasmon resonance (SPR) (4, 9, 25). This assay enables measurement of in situ dwell times below the reported detection limit of SPR measurements (9).

Direct readout of the binding status of single pMHC molecules also enables measurement of the fraction of bound pMHC within each individual T cell–supported membrane junction. In these experiments, every component of the reaction quotient ([TCR_{Total}], [pMHC:TCR], and [$pMHC_{Total}$]) is measured independently to calculate a parameter we here refer to as ${}^{cell}K_D$, which is defined as ${}^{cell}K_D = [TCR_{free}][pMHC_{free}]/[pMHC:TCR]$ and is essentially the in situ dissociation constant, K_D, within the interface (Fig. 2 *A* and *B*). Although the coreceptor CD4 is not explicitly mentioned here it is present in all measurements and is expected to weakly interact with MHC to form a CD4:pMHC:TCR ternary complex (26). All observations and calculations of ${}^{cell}K_D$ thus intrinsically include the effects of CD4 binding.

Although ${}^{cell}K_D$ is not strictly an equilibrium parameter, typical kinetic rates of binding and dissociation (k_{on} and k_{off}) are fast compared with the timescale of experiment. Under these conditions, the fraction of bound pMHC per T cell maintains at steady state during the course of observation (Fig. 2*C* and Fig. S1*A* and Movie S1). Population average values of ${}^{cell}K_D$ calculated directly from single-cell measurements are comparable to equilibrium K_D measurements obtained from parametric fits to bulk measurements of pMHC:TCR binding in supported membranes for all three pMHC:TCR combinations (Fig. 2*B* and Fig. S1*B*). There is, however, large variation in the individual values of ${}^{cell}K_D$ measured for each cell, which is not the result of measurement error or stochastic noise (Fig. 2*B*). We speculated that this variation is not random but rather reflects systematic modulation of pMHC:TCR binding characteristics by cellular activity.

Systematic Variation of pMHC:TCR Binding Affinity. The dependence of ${}^{cell}K_D$ on pMHC density was characterized by precision titrations ranging from very low pMHC densities (~0.05 molecules per micrometer) to very high pMHC densities (~300 molecules per micrometer). For a given pMHC density, ${}^{cell}K_D$ values for at least 50 cells were averaged to calculate a well-defined population average, $\langle {}^{cell}K_D\rangle$ (Fig. 3*A* and Fig. S2*A*). This assay is accurate over at least four orders of magnitude of pMHC density (Fig. S1 *C* and *D*). Several distinct observations regarding the nature of ligand:receptor binding in T cell intermembrane junctions are revealed by these results.

First, pMHC:TCR binding at the lowest densities, corresponding to as few as four to five individually resolved pMHC:TCR molecular binding events per cell (Figs. S1*B* and S2*B*), exhibits distinct positive feedback. This is revealed by the systematically decreasing values of $\langle {}^{cell}K_D\rangle$ observed at the lowest pMHC densities (Fig. 3*A* and Fig. S2*A*). The mean pMHC:TCR dwell time, $\langle\tau_{off}\rangle$, remains constant over the same pMHC density range, indicating that the pMHC:TCR k_{on} is modulated (Fig. 3*A* and Fig. S2*B*).

Second, pMHC:TCR binding exhibits positive cooperativity without physical contact between pMHC:TCR complexes. Every pMHC:TCR molecular complex is directly resolved and is observed to be spaced microns apart at the lowest pMHC densities tested (Figs. 1*B*, 2*A*, and 3*D* and Fig. S2*C*).

Third, regardless of the stimulating pMHC ligand or the T cell clone, $\langle {}^{cell}K_D\rangle$ reaches maximum affinity at the lower pMHC density ranges tested (1.35–5.75 molecules per micrometer) (Fig. S2 *A* and *B*). The density at which $\langle {}^{cell}K_D\rangle$ reaches its maximum is here referred to as the optimal pMHC density. At progressively higher pMHC densities pMHC:TCR binding exhibits negative cooperativity (Fig. 3*A* and Fig. S2*A*). Thus, under conditions at which TCR microclusters are readily observed (22, 23, 27) (Fig. S2*C*), pMHC:TCR binding is anticooperative—contrary to common assumption.

The pMHC densities at which maximum pMHC:TCR affinity is measured coincide with T cell activation thresholds for all three pMHC:TCR combinations (Fig. 3*B* and Fig. S2*A*). NFAT translocates to the nucleus in response to sustained calcium

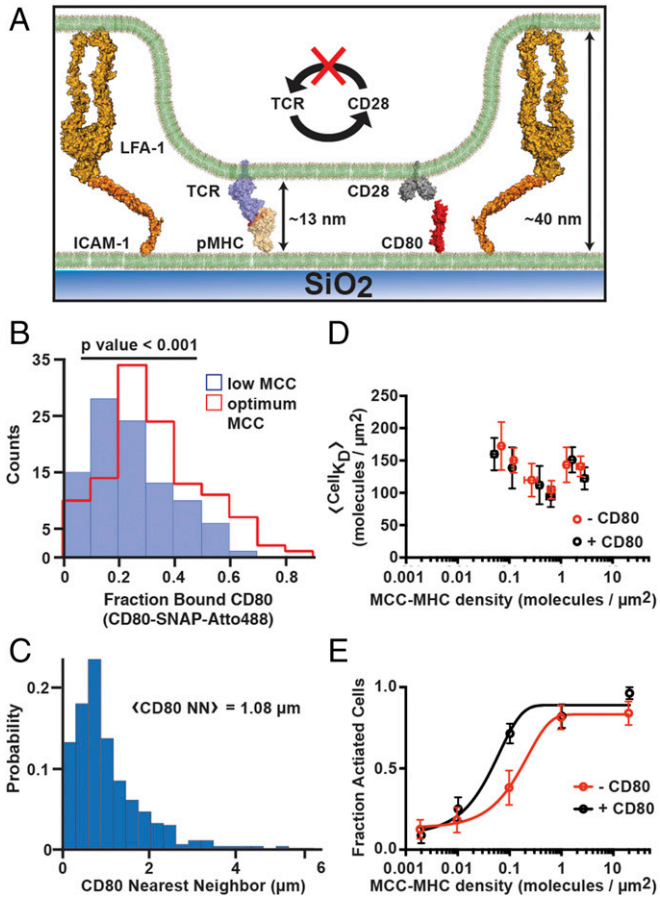

Fig. 4. pMHC:TCR feedback enhances CD80:CD28 binding. (*A*) Experimental schematic. pMHC:TCR binding enhances CD80:CD28 affinity, and this effect is not reciprocal. (*B*) CD80:CD28 binding efficiency increases when AND T cell clones are stimulated by MCC/MHC at optimal density (0.6–0.7 molecules per micrometer) relative to stimulation at low density (0.05–0.10 molecules per micrometer). A CD80-SNAP fusion is labeled 1:1 with the Atto488 fluorophore via the SNAP tag and is kept at a constant density of 0.13–0.24 CD80-SNAP per micrometer on the bilayer. MCC/MHC is unlabeled. Data from ≥100 cells from three separate mice were used to populate the histogram for each condition. (*C*) The distribution of bound CD80 nearest neighbors was calculated at 0.18 CD80-SNAP per micrometer. (*D*) Addition of unlabeled CD80 to the supported membrane (at ~200 molecules per micrometer) has a negligible effect on MCC/MHC:AND binding affinity over a range of pMHC densities. (*E*) Addition of unlabeled CD80 to the supported membrane lowers the NFAT threshold density for the MCC/MHC:AND combination. Each circle indicates a population average, and error bars show SEM. $n \geq 50$ for $^{cell}K_D$ and NFAT measurements at each condition.

release, and confocal microscopy imaging of NFAT subcellular localization provides a visual, binary readout of individual T cell activation (Fig. 3*C*). For each peptide, the activation threshold is the density at which half of the maximum fraction of cells translocate NFAT after 30 min of pMHC stimulation (28) (Fig. 3*B* and Fig. S2 *A* and *B*). At pMHC densities below the activation threshold, where T cells are scanning for and engaging antigen but have a low probability of activation (NFAT translocation), we measure positive cooperativity in pMHC:TCR binding. At higher pMHC densities, where T cells are likely to be activating, we measure negative cooperative binding between pMHC and TCR (Fig. 3 *A* and *B* and Fig. S2*A*).

Finally, the feedback strength, which is reflected in the slope of change in $\langle {}^{cell}K_D \rangle$ with pMHC density, depends on $\langle \tau_{off} \rangle$ of the stimulating ligand (Fig. S2 *A* and *B*). Thus, there is kinetic discrimination in this effect, which suggests TCR triggering is involved. Here, we refer to these TCR-mediated effects that are initiated by as few as five pMHC:TCR binding events and are insufficient to induce NFAT activation as "early TCR signals" (Fig. S2). This TCR-mediated feedback depends on pMHC:TCR strength (Fig. S2*B*), but the precise signaling pathways remain to be mapped.

TCR-Mediated Feedback Modulates CD80:CD28 Binding Affinity. Modulation of pMHC:TCR affinity occurs through changes in k_{on} of the pMHC:TCR interaction. k_{on} is a contextual parameter that is intrinsically affected by the intermembrane environment (29–31). We therefore hypothesized that the first few pMHC:TCR binding interactions could trigger changes in the T cell:APC interface, which in turn increased k_{on} of subsequent pMHC:TCR binding. Such a general morphological mechanism should also produce similar effects on other juxtacrine ligand:receptor interactions at the interface. Both CD80:CD28 and pMHC:TCR complexes have intermembrane distances of ~13 nm and bind with comparable solution affinities in the low micromolar range (25, 32–34) (Fig. 4*A*). Therefore, if a general change in membrane morphology is enhancing pMHC:TCR binding, this effect should also be experienced by other, similarly sized intermembrane ligand:receptor complexes, such as CD80:CD28.

We varied the unlabeled pMHC density and monitored single-molecule binding kinetics of the CD80:CD28 costimulatory interaction using the same imaging strategy applied to pMHC:TCR (Fig. 4*A*). Observations of individual CD80:CD28 binding events reveal a similar increase in binding efficiency at the same pMHC densities that maximized pMHC:TCR affinity for both MCC and T102S peptides (Fig. 4*B* and Fig. S3 *A* and *B*). Histograms for each condition are populated from AND CD4+ T cell clones from three separate mice. Well-resolved CD80:CD28 binding events are spaced microns apart (Fig. 4*C* and Fig. S3*C*) and their intensity distribution remains constant when pMHC density is varied (Fig. S3*C*), which demonstrates that the increase in CD80 affinity is not due to enhanced CD28:CD80 dimerization (35). Notably, this cross-talk effect of pMHC:TCR binding on CD80:CD28 affinity is not reciprocal. Addition of (unlabeled) CD80 does not appreciably shift pMHC:TCR $\langle {}^{cell}K_D \rangle$ [the difference in $\langle {}^{cell}K_D \rangle$ minima with and without CD80 (~0.15) is within the SE in the pMHC titration measurement (0.11–0.15)], indicating that CD80:CD28 binding does not contribute to the cooperative effect (Fig. 4*D*). Addition of CD80 lowers the NFAT translocation threshold density for the agonist MCC ligand (36), but this effect is less prominent for the weaker T102S ligand (Fig. 4*E* and Fig. S3*D*). CD80:CD28 complexes travel along linear trajectories, confirming effective engagement with the T cell cytoskeleton (Fig. S3*E*). Similar to pMHC:TCR, the CD80:CD28 $\langle \tau_{off} \rangle$ is constant as a function of pMHC density (Fig. S3*F*).

These results reveal that positive feedback generated by early pMHC:TCR binding events also increases k_{on} for CD80:CD28, while CD80:CD28 binding exhibits no reciprocal effect on pMHC:TCR. Since CD80:CD28 and pMHC:TCR complexes are physically similar, and are therefore expected to exert similar mechanical perturbations on the intermembrane environment, the lack of reciprocal binding cooperativity suggests a passive physical mechanism of membrane pinning is not responsible for the observed cooperativity. Instead, the mechanism appears to involve morphological changes in the interface triggered by signaling activity of pMHC:TCR.

Cytoskeleton and Integrin Signaling Contribute to pMHC:TCR Affinity Enhancement. Both pMHC:TCR and CD80:CD28 complexes clearly engage the cytoskeleton at densities below NFAT threshold where affinity enhancement is observed. Additionally, integrins play an important role in establishing the physical geometry of the intercellular interface. Both effects could modulate ligand:receptor binding, and we examine these possibilities here with inhibitor studies. We probe the role of cytoskeleton activity in pMHC:TCR affinity enhancement using the small-molecule inhibitor Latrunculin A (LatA), which disrupts actin polymerization by binding G-actin. Effects of integrin signaling were probed using GGTI-298, a geranylgeranyltransferase I

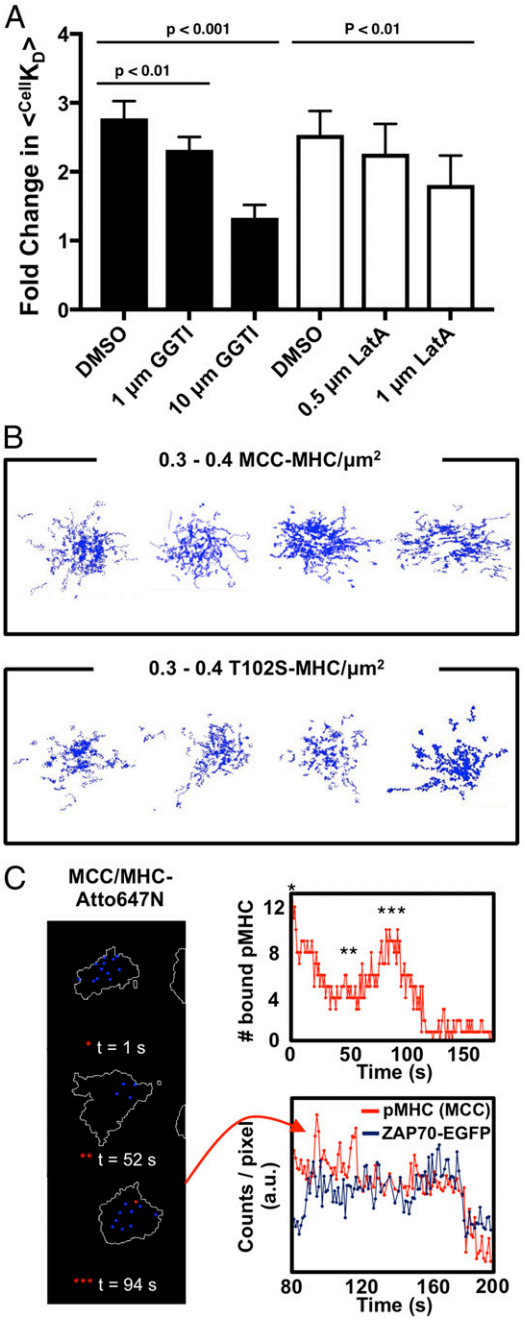

Fig. 5. Cytoskeleton and integrin signaling contribute to pMHC:TCR affinity enhancement. (*A*) The fold change in the fraction of bound MCC-Atto488/MHC at the optimum MCC density relative to the lowest MCC density decreases in the presence of Rap1 and actin inhibition for AND T cells. $n \geq 15$ for each condition. Error bars indicate SEM. (*B*) ZAP70-EGFP speckles in AND T cells are imaged using TIRF microscopy. Each blue dot represents a ZAP70-EGFP speckle; the positions of every ZAP70-EGFP feature collected over an ∼5-min window are projected onto a single image for each cell. Linear ZAP70-EGFP trajectories are visible in T cells exposed to either MCC/MHC or T102S/MHC. These trajectories are centrosymmetric in the case of MCC/MHC and asymmetric in the case of T102S/MHC. (*C*, *Left*) An AND T cell scavenges for MCC/MHC over an ∼120-s period. An edge detection algorithm using ZAP70-EGFP in TIRF as a contrast agent detects the cell outline. Individual MCC-Atto647N/MHC molecules (blue dots) are tracked in TIRF. (*C*, *Top Right*) Cell movement corresponds with an increase in pMHC binding. *, **, and *** denote time points as indicated in the images at *Left*. (*C*, *Bottom Right*) The pMHC molecule indicated by the red dot at $t = 94$ s reveals localized recruitment and correlated movement of ZAP70-EGFP at the site of pMHC:TCR binding. (Scale bar, 5 μm.)

inhibitor that targets GTPase Rap1 (37). Rap1 activates inside-out signaling via interactions with LFA-1 (21).

Dose titrations of each inhibitor were performed at pMHC densities close to and below the maximum affinity for the MCC/MHC:AND interaction (Fig. 5*A*). Titrating the dose of GGTI-298 resulted in a monotonic decrease in MCC:TCR affinity enhancement, and titrating the dose of LatA leads to a similar, but smaller, decrease in affinity enhancement. At the optimum density, phalloidin staining after T cell fixation revealed the expected enrichment of F-actin at the T cell periphery in the absence of LatA and a relatively even distribution of F-actin in the presence of LatA (Fig. S4*A*). Inclusion of a recombinant ICAM-YFP fusion in the supported membrane revealed the expected ring-like ICAM distribution at the periphery of control T cells (Fig. S4*B*). Rap1 inhibition not only disrupted this distribution of ICAM, resulting in a relatively even ICAM-YFP distribution across the T cell, but also decreased the probability of the T cell's landing on the supported membrane. These cytoskeletal and adhesion effects may be related to density- and $\langle \tau_{off} \rangle$-dependent trends in T cell landing on pMHC-conjugated supported membranes (Fig. S4*C*). Inhibition of either actin polymerization or Rap1 activity alters the pMHC:TCR affinity modulation and thus indicates a mechanistic role for both cytoskeleton and integrin inside-out signaling in pMHC:TCR affinity enhancement.

TCR-Mediated Morphology, Adhesion Dynamics, and Proximal Signaling. The decreasing trend in ${}^{cell}K_D$ before NFAT activation indicates that T cells become more responsive to their surroundings after a few initial binding events. This enhanced sensitivity is also reflected in changes in cell morphology, adhesion, and proximal signaling at pMHC densities where NFAT activation is not observed. At T102S/MHC densities well below NFAT threshold, T cells adopt an asymmetric, crawling morphology and exhibit low levels of Zeta-chain-associated protein kinase 70 (ZAP70) recruitment to the plasma membrane (Fig. 5*B* and Fig. S4*D*). Identical T cells exposed to MCC/MHC densities above NFAT translocation threshold exhibit a stationary, centrosymmetric cell morphology and enhanced ZAP70 recruitment. T cell crawling leads to binding of fresh pMHC and correlated ZAP70-EGFP recruitment in the newly engaged region of the supported membrane (Fig. 5*C*). The transition between these modes of behavior is mediated by TCR triggering and correlates with ${}^{cell}K_D$ changes reported here.

Discussion and Conclusion

Even at pMHC densities well below NFAT translocation thresholds we observe T cells to exhibit a global response to antigen that modulates the binding affinities of ligand:receptor complexes within the interface. We have previously reported that individual pMHC:TCR binding events have been observed to elicit macroscopic changes in cytoskeleton behavior (12). This effect, also readily observed in the data presented here (Fig. 1*B* and Fig. 5), illustrates how different signaling pathways triggered by the TCR can have different set points for activation. We find that, depending on the pMHC:TCR interaction and the composition of the T cell clone, at the lowest densities measured (corresponding to as few as approximately five steady-state pMHC molecular binding events per cell), T cells can activate retrograde transport of pMHC:TCR complexes and induce an increase in affinity for pMHC. Although the effects we report here are not spatially localized, this positive feedback may be enhanced by mechanisms dependent on close physical proximity of pMHC:TCR complexes (38) and by interplay between local Ca^{2+} release and actin polymerization at the supported membrane:T cell interface (39). By contrast, at densities that result in half-maximal NFAT nuclear translocation in both AND and 5c.c7 systems, T cells have at least 30 simultaneous pMHC:TCR engagement events per cell (Fig. S2*B*). Addition of the costimulatory molecule CD80 shifts NFAT triggering thresholds to lower pMHC densities (Fig. 4*E*).

The ability of T cells to respond to a small number of pMHC (here observed by modulating k_{on}) without fully activating may

provide a mechanism by which individual T cells reduce their error rate during antigen detection. This would enable T cells to transiently slow down and check for more antigen on a particular APC, or to rebind the same antigen for multiple measurements of its dwell time. The cell may keep crawling if the initial binding events do not lead to sufficient additional pMHC:TCR binding and subsequent T cell activation (Fig. 5*C*). Such a mechanism would favor efficient scanning for antigen while allowing the cell to slow for a closer look if even just a few binding events above a certain temporal threshold are detected. T cells also express over 30 costimulatory ligands, depending on the differentiation state and physical context of the T cell (40). The TCR-gated affinity enhancement observed here is likely to affect other costimulatory receptors as well.

Alternatively, it is possible that the affinity modulation we observe is a reflection of the physical mechanism of TCR signaling, without a specific physiological function of its own. The molecular interactions between TCR and its pMHC ligand are intrinsically coupled to mechanical aspects of the cell, through the cytoskeleton and the intermembrane interface. The experimental observations made here provide highly quantitative information on the in situ molecular binding events between pMHC and TCR and thus capture reflections of other features of the signaling activity. This general line of study has the ability to expose aspects of TCR signaling and T cell ligand discrimination not readily resolved by more classical experiments.

Materials and Methods

Peptides (MCC, T102S, K3, and ER60), MHC, CD80, ICAM-1, ICAM-YFP, supported membranes, and T cells were prepared as described previously (12, 36, 41). CD80 fused to decahistidine-tagged $SNAP_f$ (GenScript) was expressed in ES-sf9 cells and purified by Ni^{2+}-nitrilotriacetic acid agarose affinity (Qiagen) with 1 mM cysteine. T cells were transduced as described previously with Zap70-EGFP (12) or NFAT-GFP (42). All mouse work was approved by Lawrence Berkeley National Laboratory Animal Welfare and Research Committee under the Animal Use Protocol 17702. T cells were pretreated in suspension with Latrunculin A (Sigma) or GGTI-298 (Sigma) for 15 min or 1 h, respectively, before exposure to the lipid bilayer. Single-molecule and confocal imaging experiments were performed on separate motorized inverted microscopes as described previously (12, 43). Single-molecule data were analyzed using a custom-written particle analysis suite developed in MATLAB (The MathWorks) and NFAT data were analyzed using ImageJ (44). More detailed methods are provided in *SI Materials and Methods*.

ACKNOWLEDGMENTS. We thank David King of the Howard Hughes Medical Institute Mass Spectrometry Facility for peptide synthesis and mass spectroscopy, Art Weiss and Byron Au-Yeung for helpful feedback, and Kyle Daniels for his expertise and guidance regarding the Markov chain Monte Carlo estimation. This work was supported by NIH Grant PO1 A1091580.

1. Viola A, Lanzavecchia A (1996) T cell activation determined by T cell receptor number and tunable thresholds. *Science* 273:104–106.
2. Irvine DJ, Purbhoo MA, Krogsgaard M, Davis MM (2002) Direct observation of ligand recognition by T cells. *Nature* 419:845–849.
3. Huang J, et al. (2013) A single peptide-major histocompatibility complex ligand triggers digital cytokine secretion in CD4(+) T cells. *Immunity* 39:846–857.
4. Matsui K, Boniface JJ, Steffner P, Reay PA, Davis MM (1994) Kinetics of T-cell receptor binding to peptide/I-Ek complexes: Correlation of the dissociation rate with T-cell responsiveness. *Proc Natl Acad Sci USA* 91:12862–12866.
5. Lyons DS, et al. (1996) A TCR binds to antagonist ligands with lower affinities and faster dissociation rates than to agonists. *Immunity* 5:53–61.
6. Williams CB, Engle DL, Kersh GJ, Michael White J, Allen PM (1999) A kinetic threshold between negative and positive selection based on the longevity of the T cell receptor-ligand complex. *J Exp Med* 189:1531–1544.
7. Daniels MA, et al. (2006) Thymic selection threshold defined by compartmentalization of Ras/MAPK signalling. *Nature* 444:724–729.
8. Stone JD, Chervin AS, Kranz DM (2009) T-cell receptor binding affinities and kinetics: Impact on T-cell activity and specificity. *Immunology* 126:165–176.
9. Corse E, Gottschalk RA, Krogsgaard M, Allison JP (2010) Attenuated T cell responses to a high-potency ligand in vivo. *PLoS Biol* 8:e1000481.
10. Huppa JB, et al. (2010) TCR-peptide-MHC interactions in situ show accelerated kinetics and increased affinity. *Nature* 463:963–967.
11. Huang J, et al. (2010) The kinetics of two-dimensional TCR and pMHC interactions determine T-cell responsiveness. *Nature* 464:932–936.
12. O'Donoghue GP, Pielak RM, Smoligovets AA, Lin JJ, Groves JT (2013) Direct single molecule measurement of TCR triggering by agonist pMHC in living primary T cells. *eLife* 2:e00778.
13. McKeithan TW (1995) Kinetic proofreading in T-cell receptor signal transduction. *Proc Natl Acad Sci USA* 92:5042–5046.
14. Rabinowitz JD, Beeson C, Lyons DS, Davis MM, McConnell HM (1996) Kinetic discrimination in T-cell activation. *Proc Natl Acad Sci USA* 93:1401–1405.
15. François P, Voisinne G, Siggia ED, Altan-Bonnet G, Vergassola M (2013) Phenotypic model for early T-cell activation displaying sensitivity, specificity, and antagonism. *Proc Natl Acad Sci USA* 110:E888–E897.
16. Chakraborty AK, Weiss A (2014) Insights into the initiation of TCR signaling. *Nat Immunol* 15:798–807.
17. Dushek O, van der Merwe PA (2014) An induced rebinding model of antigen discrimination. *Trends Immunol* 35:153–158.
18. Grakoui A, et al. (1999) The immunological synapse: A molecular machine controlling T cell activation. *Science* 285:221–227.
19. Mossman KD, Campi G, Groves JT, Dustin ML (2005) Altered TCR signaling from geometrically repatterned immunological synapses. *Science* 310:1191–1193.
20. Salaita K, et al. (2010) Restriction of receptor movement alters cellular response: Physical force sensing by EphA2. *Science* 327:1380–1385.
21. Springer TA, Dustin ML (2012) Integrin inside-out signaling and the immunological synapse. *Curr Opin Cell Biol* 24:107–115.
22. Campi G, Varma R, Dustin ML (2005) Actin and agonist MHC-peptide complex-dependent T cell receptor microclusters as scaffolds for signaling. *J Exp Med* 202:1031–1036.
23. Varma R, Campi G, Yokosuka T, Saito T, Dustin ML (2006) T cell receptor-proximal signals are sustained in peripheral microclusters and terminated in the central supramolecular activation cluster. *Immunity* 25:117–127.
24. Valitutti S, Müller S, Cella M, Padovan E, Lanzavecchia A (1995) Serial triggering of many T-cell receptors by a few peptide-MHC complexes. *Nature* 375:148–151.
25. Newell EW, et al. (2011) Structural basis of specificity and cross-reactivity in T cell receptors specific for cytochrome c-I-E(k). *J Immunol* 186:5823–5832.
26. Yin Y, Wang XX, Mariuzza RA (2012) Crystal structure of a complete ternary complex of T-cell receptor, peptide-MHC, and CD4. *Proc Natl Acad Sci USA* 109:5405–5410.
27. Yokosuka T, et al. (2005) Newly generated T cell receptor microclusters initiate and sustain T cell activation by recruitment of Zap70 and SLP-76. *Nat Immunol* 6:1253–1262.
28. Marangoni F, et al. (2013) The transcription factor NFAT exhibits signal memory during serial T cell interactions with antigen-presenting cells. *Immunity* 38:237–249.
29. Hu J, Lipowsky R, Weikl TR (2013) Binding constants of membrane-anchored receptors and ligands depend strongly on the nanoscale roughness of membranes. *Proc Natl Acad Sci USA* 110:15283–15288.
30. Bihr T, et al. (2014) Association rates of membrane-coupled cell adhesion molecules. *Biophys J* 107:L33–L36.
31. Bihr T, Seifert U, Smith AS (2012) Nucleation of ligand-receptor domains in membrane adhesion. *Phys Rev Lett* 109:258101.
32. Evans EJ, et al. (2005) Crystal structure of a soluble CD28-Fab complex. *Nat Immunol* 6:271–279.
33. van der Merwe PA, Bodian DL, Daenke S, Linsley P, Davis SJ (1997) CD80 (B7-1) binds both CD28 and CTLA-4 with a low affinity and very fast kinetics. *J Exp Med* 185:393–403.
34. Sharpe AH, Freeman GJ (2002) The B7-CD28 superfamily. *Nat Rev Immunol* 2:116–126.
35. Sanchez-Lockhart M, et al. (2014) T cell receptor signaling can directly enhance the avidity of CD28 ligand binding. *PLoS One* 9:e89263.
36. Manz BN, Jackson BL, Petit RS, Dustin ML, Groves J (2011) T-cell triggering thresholds are modulated by the number of antigen within individual T-cell receptor clusters. *Proc Natl Acad Sci USA* 108:9089–9094.
37. Muramatsu R, et al. (2011) RGMa modulates T cell responses and is involved in autoimmune encephalomyelitis. *Nat Med* 17:488–494.
38. Taylor MJ, Husain K, Gartner ZJ, Mayor S, Vale RD (2017) A DNA-based T Cell receptor reveals a role for receptor clustering in ligand discrimination. *Cell* 169:108–119.e20.
39. Hartzell CA, Jankowska KI, Burkhardt JK, Lewis RS (2016) Calcium influx through CRAC channels controls actin organization and dynamics at the immune synapse. *eLife* 5:e14850.
40. Chen L, Flies DB (2013) Molecular mechanisms of T cell co-stimulation and co-inhibition. *Nat Rev Immunol* 13:227–242.
41. Hartman NC, Nye JA, Groves JT (2009) Cluster size regulates protein sorting in the immunological synapse. *Proc Natl Acad Sci USA* 106:12729–12734.
42. Morita S, Kojima T, Kitamura T (2000) Plat-E: An efficient and stable system for transient packaging of retroviruses. *Gene Ther* 7:1063–1066.
43. Greene AC, et al. (2014) Spatial organization of EphA2 at the cell-cell interface modulates trans-endocytosis of ephrinA1. *Biophys J* 106:2196–2205.
44. Schneider CA, Rasband WS, Eliceiri KW (2012) NIH Image to ImageJ: 25 years of image analysis. *Nat Methods* 9:671–675.
45. Edelstein A, Amodaj N, Hoover K, Vale R, Stuurman N (2010) Computer control of microscopes using μmanager. *Curr Protoc Mol Biol* 92:14.20:14.20.1–14.20.17.
46. Daniels KG, et al. (2014) Ligand concentration regulates the pathways of coupled protein folding and binding. *J Am Chem Soc* 136:822–825.
47. Crocker JC, Grier DG (1996) Methods of digital video microscopy for colloidal studies. *J Colloid Interface Stud* 310:298–310.
48. Ensign DL, Pande VS (2010) Bayesian detection of intensity changes in single molecule and molecular dynamics trajectories. *J Phys Chem B* 114:280–292.